JACS
JOURNAL OF THE AMERICAN CHEMICAL SOCIETY

Article

pubs.acs.org/JACS

π-Conjugated Heterotriangulene Macrocycles by Solution and Surface-supported Synthesis toward Honeycomb Networks

Florian Schlütter,[†] Frédéric Rossel,[‡] Milan Kivala,[†] Volker Enkelmann,[†] Jean-Paul Gisselbrecht,[§] Pascal Ruffieux,[‡] Roman Fasel,*[,‡,∥] and Klaus Müllen*[,†]

[†]Max-Planck-Institute for Polymer Research, Ackermannweg 10, D-55128 Mainz, Germany

[‡]Empa, Swiss Federal Laboratories for Materials Science and Technology, Nanotech@surfaces Laboratory, Ueberlandstrasse 129, CH-8600 Duebendorf, Switzerland

[∥]Departement für Chemie und Biochemie, Universität Bern, Freiestraße 3, CH-3012 Bern, Switzerland

[§]Laboratoire d'Electrochimie et de Chimie Physique du Corps Solide, Institut de Chimie - UMR 7177, C.N.R.S. Université de Strasbourg, 4, rue Blaise Pascal, 67000 Strasbourg, France

Supporting Information

ABSTRACT: A comparative analysis between a solution and a surface-mediated synthesis of heterotriangulene macrocycles is reported. The results show a preferential formation of the π-conjugated macrocycles on surface due to two-dimensional confinement. The macrocycle prepared on a several hundred milligram scale by solution chemistry was characterized by single-crystal X-ray analysis and was furthermore extended toward next generation honeycomb species. Investigation of the photophysical and electronic properties together with the good thermal stability revealed the potential of **MC6** as hole-transport material for organic electronics.

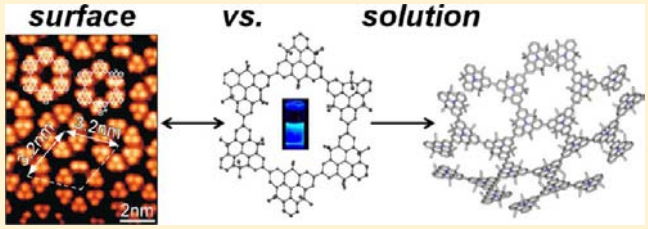

INTRODUCTION

Macrocycles with shape-persistent π-conjugated arene backbones gained tremendous interest in the last years owing to their unusual optoelectronic properties and role as building-blocks of columnar one-dimensional (1D) nanotubes, two-dimensional (2D) polymer networks and three-dimensional (3D) inclusion complexes.[1−9] Due to their monodisperse structures based on an infinite and well-defined chain without perturbing end-effects, π-conjugated macrocycles allow for reliable estimation of structure−property relationships.[7,8,10−14] In particular macrocycles bearing redox-active centers, for example, nitrogen, are useful for organic electronics and molecular switches due to changes of charge and shape upon redox processes.[9,15]

Exploring these materials is often hampered by their challenging and low yielding syntheses, a result of the preferential formation of acyclic oligomers. Highly diluted reaction mixtures were utilized to support entropically unfavored cyclization and to suppress intermolecular aryl−aryl coupling in the final step.[1,2] Synthesizing preorganized building blocks and applying template-directed cyclizations increased the yields and gave macrocycles with larger cavities.[3,4,7,8,16−22]

An alternative opportunity is on-surface reactions of confined molecular precursors.[23−26] Recently it has been shown that surface-mediated syntheses afford molecular nanostructures such as, ultranarrow graphene nanoribbons,[27] honeycomb networks,[28−31] poly(phenylene) and poly(fluorene) nanowires[32,33] or transition metal phthalocyanine sheets.[34] Advantages of the on-surface synthesis under ultrahigh vacuum (UHV) conditions are a much broader temperature range providing access to new reaction pathways not observed in solution chemistry. Furthermore, scanning tunneling microscopy (STM) allows imaging at a submolecular level and thus a straightforward *in situ* characterization.[23,35,36]

We have fabricated molecular-thin 2D covalently linked polymers based on dimethylmethylene-bridged triphenylamines (DTPA), so-called heterotriangulenes,[37−40] on metal surfaces.[31] Due to their good hole-transport properties and often large two-photon absorption, such triphenylamines gained significant interest in optoelectronic applications in the last decades.[41−44] Subsequent computational studies of the 2D covalently linked heterotriangulene polymer revealed a ferromagnetic half-metal character with a semiconducting channel of 1 eV which makes it interesting for spin-selective conductors.[45] The aesthetically appealing structure of the observed honeycomb network (Figure 1) motivated us to design easy ways for the synthesis of its macrocyclic subunits and their expanded fragments. Moreover, the cyclic arrangement of the DTPA units raises the question to which extent the photophysical properties, for example, photoluminescence quantum yields (PLQY) will be altered compared to the DTPA monomer. Different from linear or dendritic triarylamines, the cyclic structure will change structural features, which may improve the molecular ordering in the solid state and enhance the charge carrier transport in organic

Received: January 25, 2013
Published: February 25, 2013

   dx.doi.org/10.1021/ja400857g | J. Am. Chem. Soc. 2013, 135, 4550−4557

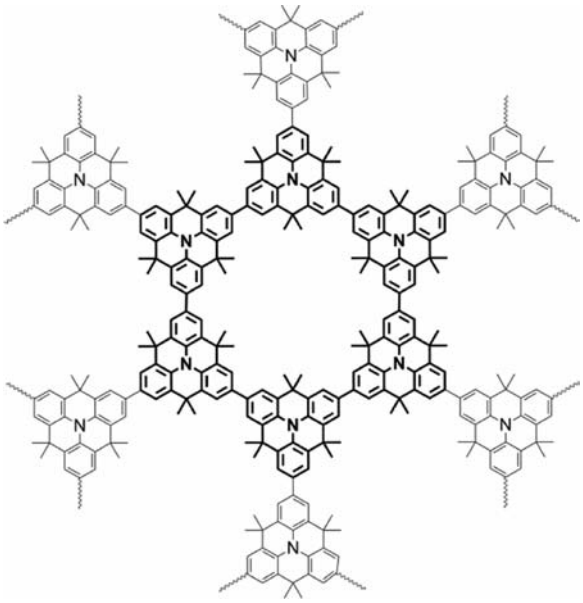

Figure 1. Structure of a fraction of the honeycomb structured DTPA polymer observed on surface. The macrocyclic subunit is highlighted.

electronics.[46] Toward this end, we present here a comparative study of solution-based and surface-mediated syntheses of an unprecedented π-conjugated macrocycle consisting of electron-rich heterotriangulene moieties together with its hyperbranched expansions. We discuss the effect of cyclization on the photophysical and electronic characteristics and present the single crystal X-ray structure of the DTPA macrocycle.

EXPERIMENTAL SECTION

Materials, methods, detailed synthetic procedures and characterization data for compounds DTPA, **1**−**6**, **MC6**, **G1**, **G2** and **L9** as well as complete information about the STM experiments can be found in the Supporting Information.

RESULTS AND DISCUSSION

We first aimed at a direct synthesis of the DTPA macrocycle (**MC6**, Scheme 1c) from a bis-functionalized DTPA building block (**1a** or **1b**) by applying transition-metal mediated coupling procedures in solution (Scheme 1a). Both *Yamamoto* coupling of dibromo-substituted DTPA **1a** and Suzuki-Miyaura cross-coupling of bromo-boronate **1b** afforded similar results, providing complex mixtures of acyclic oligomers with up to 10 DTPA units (see the Supporting Information). The isotopic pattern of the hexameric peak (n = 6, m/z = 2181) revealed two distributions with a mass difference of two Dalton, corresponding to the DTPA macrocycle and the linear hexamer. To quantify the amount of **MC6** formed during the one-step reaction, we enriched the hexameric fraction by means of repeated preparative size-exclusion chromatography (SEC). Judging from the broadened and less distinct signals of the ^{1}H NMR spectrum, the obtained yield of macrocycle **MC6** is below 5% (see the Supporting Information), which was not improved by altering the concentration of the monomer.

To compare these results with a surface-mediated synthesis, we fabricated heterotriangulene oligomers on an atomically flat Ag(111) surface using the dibromo-substituted DTPA **1a**. This approach could potentially lead to zigzag oligomers (Scheme 1b), six-membered macrocycles (Scheme 1c) and mixed chains (Scheme 1d), in agreement with the results of our solution

Scheme 1. One-step Synthesis to Macrocycle MC6[a]

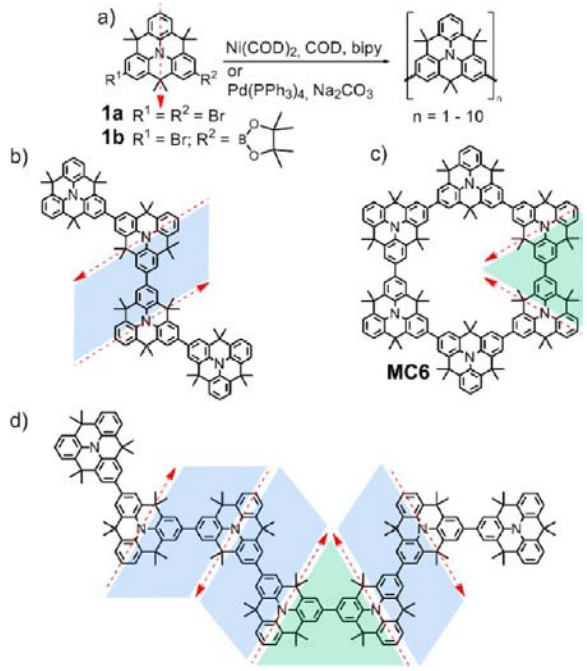

[a](a) Solution based one-step synthesis toward **MC6** from difunctionalized DTPAs (**1a** or **1b**). The molecular main axis is indicated by a dashed red arrow. COD = 1,5-cyclooctadiene, bipy = 2,2′-bipyridine. (b) Structure of a zigzag oligomer. Two monomers are linked in the zigzag configuration if their two main axes are antiparallel (blue parallelogram). (c) Structure of a six-membered macrocycle. Two monomers are linked in the cycle configuration if their two main axes differ by 60° (green triangle). (d) Mixed chain with links in the zigzag and cycle configurations.

attempts. The molecules were sublimed in ultrahigh vacuum onto the substrate held at room temperature, followed by thermal annealing at 570 K to activate the surface-promoted aryl−aryl coupling reaction.[30,31] STM topographs reveal extended nanostructures that spread across the metal surface (Figure 2a). The monomers adopt a triangular shape with bright protrusions at the edges (Figure 2b−d), which are identified as the perpendicular oriented methyl groups in agreement with previous reports.[31] The relatively high annealing temperature occasionally results in methyl scission (see e.g. the species indicated by a red arrow in Figure 2c).[31] As expected from the ditopic nature of **1a**, the formed nanostructures are essentially composed of monomers that are linked to two neighbors via covalent bonds. Occasionally the formation of three covalent bonds is observed (8 ± 1% of the monomers). The third bond is formed between the C−Br and the H−C of a phenyl moiety (see e.g. the one indicated by a green arrow in Figure 2c), which exclusively occurs on the surface. In this particular case, a carbon radical appears to attack a C−H bond of the neighboring molecule, leading to C−H bond scission and intermolecular C−C bond formation. Line profile analysis across the molecules reveals an apparent height of 0.25 nm and a center-to-center distance of 1.0 nm along the virtual Br−Br axis, confirming the covalent linking of the DTPA species (white arrow in Figure 2c).[31]

The on-surface oligomerization of **1a** on Ag(111) also leads to a significant amount of six-membered DTPA macrocycles (**MC6**), in contrast to the solution based one-step synthesis (see above). These macrocycles are frequently grouped together

dx.doi.org/10.1021/ja400857g | J. Am. Chem. Soc. 2013, 135, 4550−4557

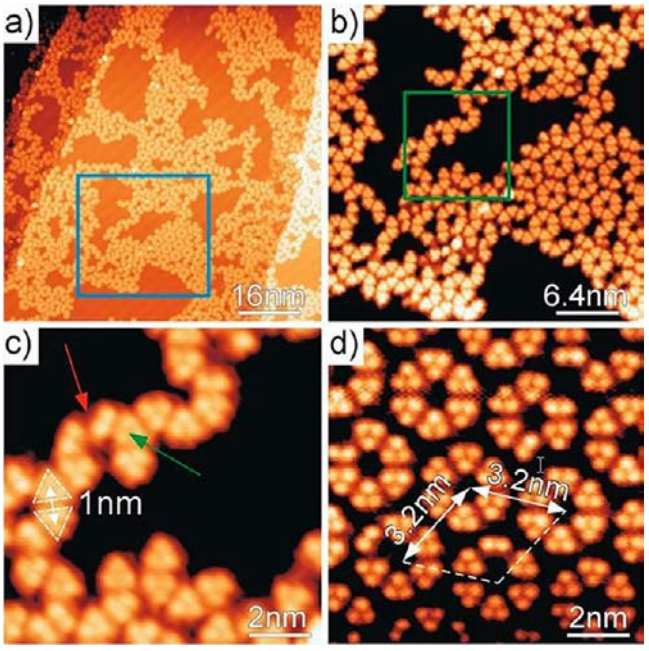

Figure 2. STM topographs (recorded at 30 K) of covalently linked DTPA nanostructures. (a) Flat oligomeric structures and macrocycles are observed. (b) Close-up view of the area highlighted by the blue rectangle in (a) revealing submolecular contrast. (c) Zoom into the green rectangle of (b). The center-to-center distance between two covalently bonded monomers is 1.0 nm. The red arrow points to a molecule with one missing methyl unit. The green arrow points to a molecule with three neighbors. (d) Island consisting of aggregated six-membered macrocycles. The distance between macrocycles is 3.2 nm. Tunneling parameters: (a) $V = -1.5$ V, $I = 0.02$ nA; (b) $V = -1.5$ V, $I = 0.02$ nA; (c) $V = -1.5$ V, $I = 0.02$ nA; (d) $V = -1.5$ V, $I = 0.05$ nA.

into ordered islands with a distance between macrocycles of about 3.2 nm (Figure 2d).

Analysis of 5 high-resolution STM images (corresponding to a total of 1937 molecules) reveals that 16 ± 2% of the monomers belong to macrocyclic species. Note that regarding this on-surface oligomerization probability of forming macrocycles both "free" six-membered macrocycles (see Figure 2d) and those anchored to one or several species via covalent linkage (see e.g. Figure 2b) were taken into account. The simplest stochastic model in which a macrocycle is built "monomer after monomer" gives a probability of only $(0.5)^4 = 6.25\%$ (two possible orientations per added molecule, whereas only one of them is leading to a macrocycle; a probability of 1 for the last monomer to close the macrocycle owing to the high chemical reactivity of the radicals). This indicates that the on-surface oligomerization is not a random process, and that the two possible orientations correspond to different reaction probabilities. By determining the "monomer main axis" of the species (Scheme 1, dashed red arrow) and using the fact that two successive monomers can be said to be linked in the cyclic (zigzag) configuration if their two axes differ by 60° (180°) (see Scheme 1b–c), we find a preference for bond formation in the cyclic configuration (60 ± 5% vs 40 ± 4%), contrary to our solution based results showing mainly acyclic oligomers.

Analyzing the results of both concepts, the superiority of the surface synthesis for obtaining **MC6** over acyclic oligomers can be concluded. Once a hexamer in the appropriate conformation has been formed in solution, it can either undergo the intramolecular aryl–aryl coupling or connect to a new monomer by rotating about the $C(sp^2)–C(sp^2)$ single bond with an equal probability of both processes. On the metal, however, essentially no such conformational changes are possible, for example, induced by the binding energy of the DTPA molecules to the Ag(111) surface. This considerably reduces the possible relative orientations of the reacting molecules, increases the intermolecular coupling probability and lowers the entropic penalty upon chain-end connection.

The fact that the covalent bond formation on Ag(111) is not random, however, is not yet fully understood. It is known that atoms in the metal surface layer are lifted up from their initial equilibrium position during the first steps that lead to the aryl–aryl coupling between the radicals.[30,47] This radical-induced surface reconstruction, as well as the related modification of the energy landscape for additional monomers, may play a crucial role regarding preferences for specific binding motifs.

In order to obtain macroscopic quantities of **MC6**, the solution-based synthesis was extended to a stepwise approach (Scheme 2). The synthesis started with a bromination/borylation sequence of DTPA to give **2**. Subsequent monobromination led to building block **3**. The Suzuki-Miyaura cross-coupling with diiodo DTPA **4** was conducted selectively below 70 °C to yield trimer **5**.[4] As expected, the concentration of **5** strongly influenced the yield of this cyclization. The cyclodimerization to yield **MC6** was achieved following standard Yamamoto conditions.[48,49] Hence, the Ni^0-complex was prepared under glovebox conditions, activated and then the solution containing trimer **5** was added slowly to ensure pseudo high-dilution conditions providing finally the hexameric macrocycle **MC6** in 38% yield on a several hundred milligram scale. A linear DTPA nonamer **L9** was obtained as byproduct in 15% yield, during purification of **MC6** by preparative SEC.

The identity of **MC6** was confirmed by mass spectrometry (high-resolution ESI MS and MALDI-TOF MS), NMR spectroscopy and SEC analysis.

HR MS confirmed the successful cyclization of **MC6** with a single signal at m/z 2180.2009 ($C_{162}H_{150}N_6$, calculated 2180.2000, see the Supporting Information). Corresponding to its highly symmetric structure, a set of sharp aromatic signals at 7.07, 7.41, and 7.69 ppm were observed in the ^{1}H NMR spectrum, which were clearly assigned to the respective protons of **MC6** (Figure 3 left).

Single crystals suitable for X-ray analysis of **MC6** indicate the successful ring closure (Figure 4a).[50] Macrocyle **MC6** deviates from planarity and the DTPA units are tilted to each other, as characterized by the dihedral angles between the single moieties ranging from 13.8(9)° to 35.5(4)°. The sum of the three C–N–C angles (358.4(5)°) revealed almost planar DTPA units as obviously no significant pyramidalization of the nitrogen takes place. In addition, the diameter of the inner cavity was found to be 14.09 Å. Crystal packing of **MC6** is shown in Figure 4b and c. It crystallizes in the centrosymmetric space group $C2/c$ as a chloroform solvate (four molecules per unit cell) and contains four macrocyles in the unit cell. The molecules are arranged in an edge-on orientation, in which every second macrocycle is placed parallel to the other. Examination of intermolecular interactions show short distances of 3.84 Å between two cycles (Figure 4b, red arrows). The steric demand of the bridging methyl groups results in an overall bent structure of the macrocycle (Figure 4c).

Thermal analysis using differential scanning calorimetry (DSC, see the Supporting Information) revealed no glass transition temperature or any melting and crystallization processes for **MC6**. Additionally thermogravimetric analysis

dx.doi.org/10.1021/ja400857g | J. Am. Chem. Soc. 2013, 135, 4550–4557

Scheme 2. Schematic Representation of the Stepwise Approach Towards MC6[a]

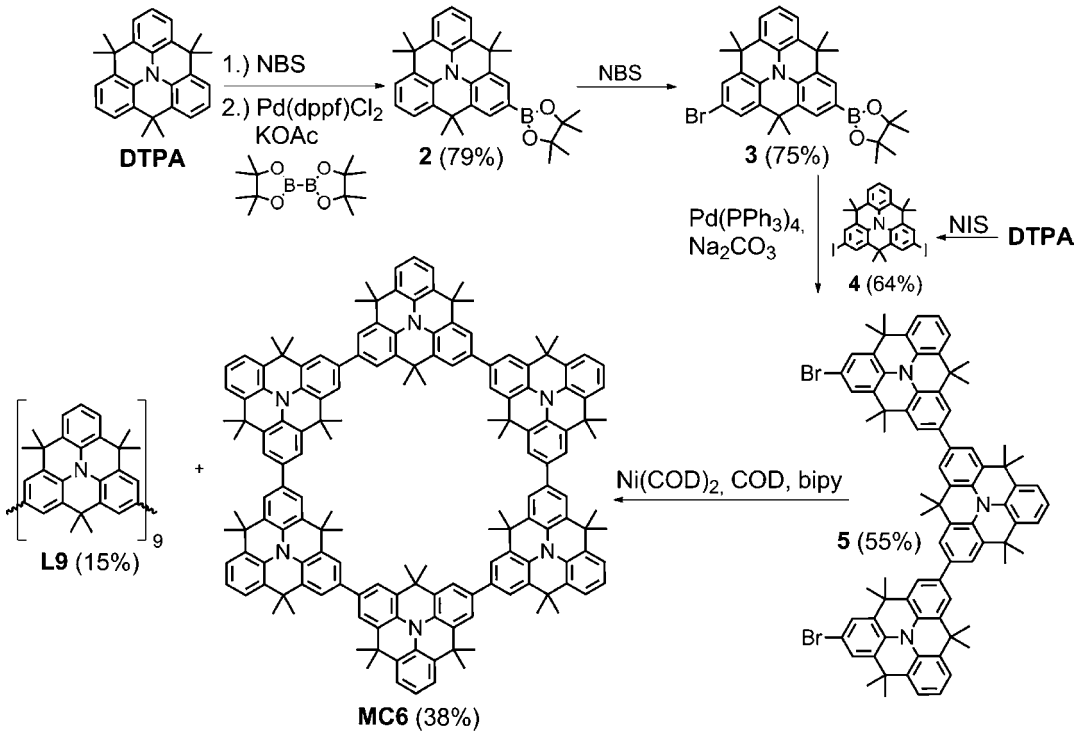

[a]COD = 1,5-cyclooctadiene, bipy =2,2′-bipyridine, NIS = *N*-iodosuccinimide, NBS = *N*-bromosuccinimide, dppf =1,1′-bis(diphenylphosphino)-ferrocene

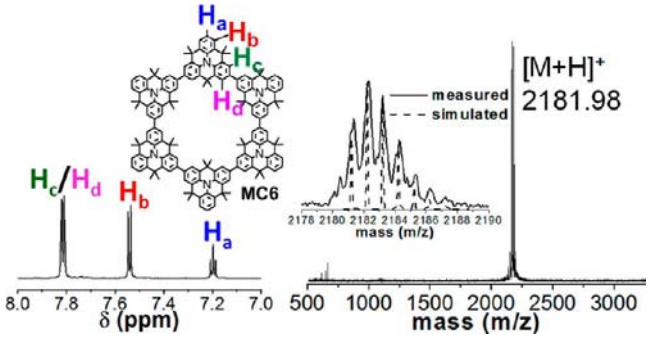

Figure 3. (Left) ^{1}H NMR of **MC6** (aromatic region, THF-d_8, 700 MHz). (Right) MALDI-TOF MS of **MC6** with the calculated and measured isotopic pattern (inset). Besides the $[M + H]^+$ peak, the scission of methyl groups depending on the power of the applied desorption laser was observed.

(TGA, see the Supporting Information) showed excellent thermal stability of **MC6** up to 400 °C (decomposition temperature at 5% weight loss is 455 °C). Considering these aspects together with the good solubility in organic solvents, for example, CH_2Cl_2, THF, toluene or 1,2-dichlorobenzene, **MC6** shows potential for good processability and a high device durability in optoelectronic applications as organic light emitting diodes (OLEDs) and field-effect transistors (FETs).

In order to get further insight into the macroscopic properties of the DTPA honeycomb structures, we were aiming at the construction of higher homologues of **MC6**. The bromination of its six peak positions, allowed for the expansion of the macrocyclic core toward higher branched architectures (Scheme 3). By utilizing Buchwalds ligand S-Phos in Suzuki-Miyaura cross-coupling under microwave irradiation, six additional DTPA units were attached to give the first generation expanded macrocycle **G1** in a considerably good overall yields (26% overall yield over two steps).[51,52] The higher generation macrocycle **G2** was synthesized in a similar protocol with boronic ester trimer **6** as the coupling partner, however, the steric demand decreased the yield of the Suzuki-Miyaura reaction (12% overall yield over two steps, see the Supporting Information).

The successful formation of **G1** and **G2** was confirmed by mass spectrometry (MALDI-TOF MS, Figure 5 bottom) and NMR spectroscopy. However, the identification by high-resolution ESI MS was only feasible for **G1** due to a decreased ionization tendency of **G2** under the applied method.

As a result of the symmetric nature of **G1** and **G2**, sharp sets of aromatic signals were observed, which could be assigned to the respective protons (Figure 5 top, see the Supporting Information). This together with the clearly separated methyl proton signals, proved the 6-fold attachment of **2** and **6** to the central macrocycle **MC6**.

Due to the amorphous nature as a result of the large size of **G1** and **G2**, single crystals suitable for X-ray analysis could not be grown.

Both compounds showed good solubility in organic solvents, for example, CH_2Cl_2, THF, toluene or 1,2-dichlorobenzene. Furthermore, no decomposition was observed after several months in the presence of light and oxygen.

The photophysical properties of **MC6**, **G1** and **G2** were investigated and compared with the DTPA subunit and the linear oligomer **L9** (Figure 6, Table 1). **MC6** exhibits two characteristic UV−vis absorption bands at 324 and 377 nm, respectively. The longest-wavelength absorption corresponds thereby to the $\pi-\pi^*$ transition of the whole π-conjugated macrocycle (DTPA, $\lambda_{abs,max}$ = 301 nm).[53−57] By extending the π-conjugation toward **G1** and **G2**, this transition is bathochromically shifted of about 17 and 7

dx.doi.org/10.1021/ja400857g | J. Am. Chem. Soc. 2013, 135, 4550−4557

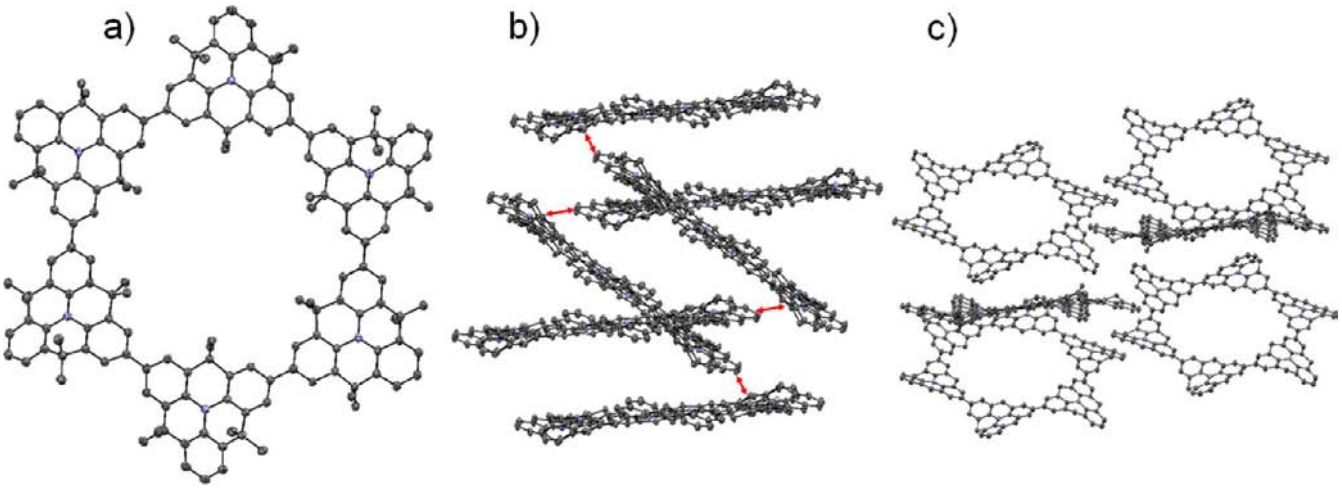

Figure 4. X-ray crystal structure of **MC6**. (a) Top view (nitrogen atoms in blue, carbon atoms in gray, hydrogens omitted for clarity). (b) Side view of the asymmetric unit. The red arrows indicate the shortest distance between two macrocycles of 3.84 Å (hydrogens and methyl-groups omitted for clarity). (c) Front view of the asymmetric unit (hydrogens and methyl-groups omitted for clarity).

Scheme 3. Schematic Representation of the Extension of MC6[a]

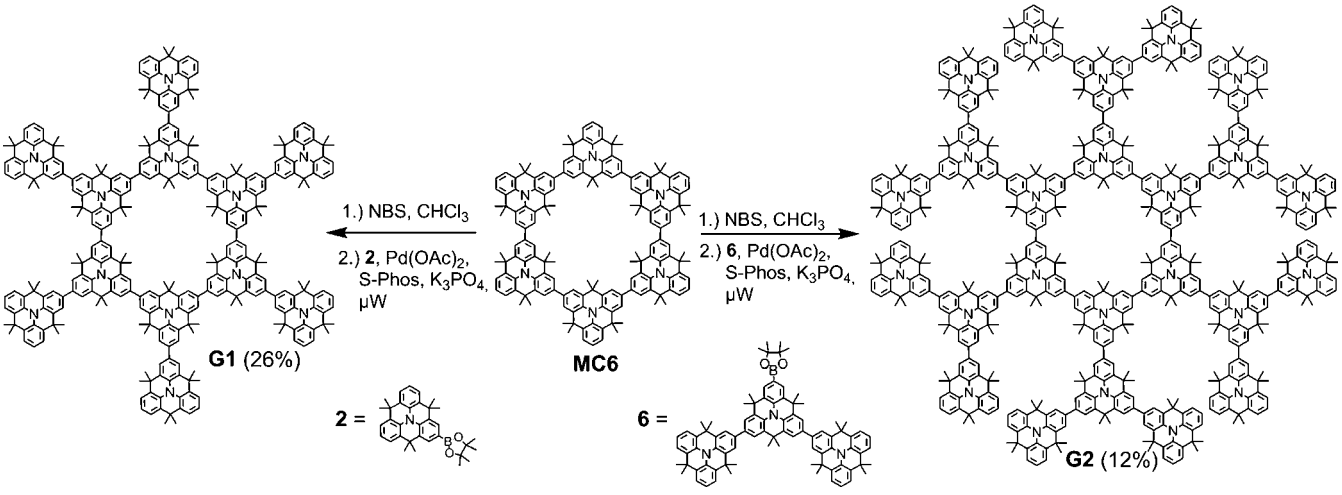

[a]Given yields are overall yields (two reaction steps). NBS = *N*-bromosuccinimide, S-Phos = 2-dicyclohexylphosphino-2′,6′-dimethoxybiphenyl.

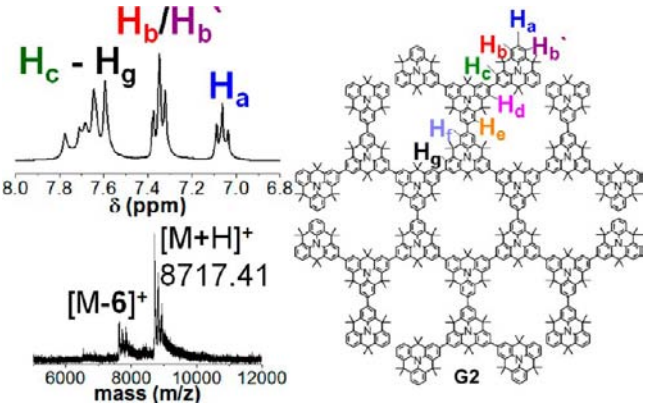

Figure 5. (Top) ^{1}H NMR of **G2** (aromatic region, CD_2Cl_2, 700 MHz). (Bottom) MALDI-TOF MS of **G2**. Besides the $[M + H]^+$ peak, the scission of methyl groups and one trimer depending on the power of the applied desorption laser was observed.

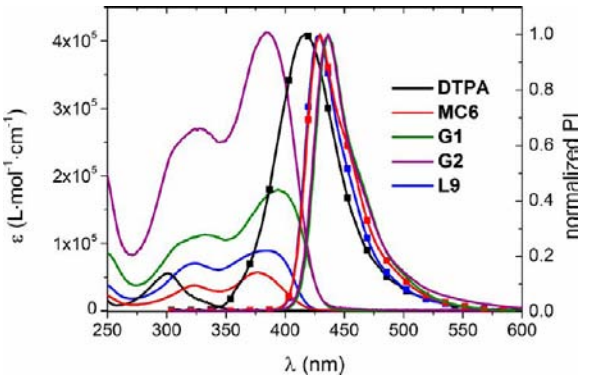

Figure 6. UV−vis absorption (solid line) and emission (symbol line) spectrum of DTPA (black), **MC6** (red), **G1** (green), **G2** (violet) and **L9** (blue). For all spectra: 10^{-6} M in CH_2Cl_2.

nm, respectively, followed by a gradually increased extinction coefficient. The observed hypsochromic shift of the longest wavelength absorption in **G2** compared with **G1** can be explained by reduced π-conjugative interactions of the macrocyclic core with the trimeric arms induced by a significant twisting upon steric repulsion. The linear oligomer **L9** ($\lambda_{abs,max}$ =

dx.doi.org/10.1021/ja400857g | J. Am. Chem. Soc. 2013, 135, 4550−4557

Table 1. Selected Photophysical and Electrochemical Data of DTPA, MC6, G1, G2 and L9

	$\lambda_{abs,max}$ [a] (nm)	$\lambda_{PL,max}$ [a,b] (nm)	Stokes shift (cm^{-1})	E_g^{opt} [c] (eV)	Φ_{PL} [a,d]	E°_{ox} [e] (V)	HOMO[f] (eV)	LUMO[g] (eV)
DTPA	301	416	9180	3.59	0.02	+0.34, +1.36	−5.14	−1.56
MC6	324, 377	430	3270	2.96	0.89	+0.14, +0.26, +0.39, +0.54	−4.94	−1.98
G1	333, 394	436	2440	2.87	0.79	+0.12, +0.30, +0.41, +0.58	−4.92	−2.05
G2	324, 384	436	3110	2.91	0.53	[h]	[h]	[h]
L9	312, 383	430	2850	2.95	0.87			

[a]For all spectra: 10^{-6} M in CH_2Cl_2. [b]Excited at the absorption maxima. [c]$E_g^{opt} = h \times c/\lambda_{0.1max}$. [d]Absolute PL quantum yields, uncorrected with respect to reabsorption. [e]Redox potentials from CV are reported vs Fc/Fc^+ (0.1 M nBu_4NPF_6 in CH_2Cl_2, scan rate 100 mV s^{-1}). [f]HOMO levels were calculated from the measured first oxidation potential. [g]LUMO levels were calculated from the optical band gap E_g^{opt} and the respective HOMO levels. [h]Owing to the small amount obtained for **G2**, an electrochemical characterization was impeded.

383 nm) featured similar transitions with a slight bathochromic shift for the longest-wavelength absorption compared with **MC6**, attributed to an extended π-conjugation length and a more restricted conformation of **MC6**. This is, however, compensated by a planarization of the π-conjugated system of the macrocycle in the excited state and thus a geometrical rearrangement, revealed by the same emission maxima ($\lambda_{PL,max}$ = 430 nm) and a comparably large Stokes shift (3270 cm^{-1}) in contrast to **L9** (2850 cm^{-1}). This geometrical rearrangement is similarly observed for **G2** (3110 cm^{-1}). Comparing the PLQY, Φ_{PL}, of 2% for parent DTPA to these of **MC6**, **G1** and **G2** up to a forty-fold improvement in the PLQY can be observed. Moreover, the macrocyclic arrangement results in a remarkable PLQY for **MC6** of 89%. These results confirm an increase in the oscillator strength of the emissive transition due to an effectively broken overall symmetry of the DTPA unit by a cyclic π- conjugated arrangement of **MC6**, while the transition energy (emission maxima) is only marginally changed.

Investigation of the redox properties of the macrocyclic species **MC6** and **G1** by cyclic voltammetry (CV) gave well resolved voltammograms showing only oxidation peaks (Figure 7 and

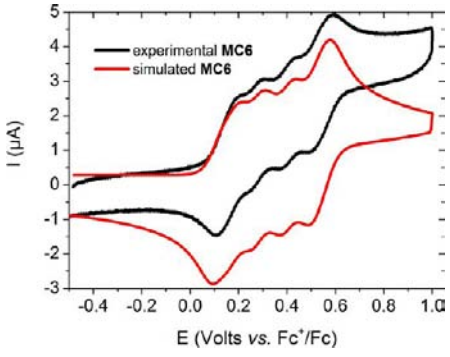

Figure 7. Cyclic voltammetry curve of **MC6** (scan rate = 0.1 V s^{-1}, black line) and its simulation using DigiElch v 6F (red line).[58]

Table 1, see the Supporting Information). Four nitrogen-centered oxidation steps could be observed for **MC6**. From the peak amplitudes, as well as the limiting currents observed by rotating disc voltammetry (RDV, see the Supporting Information), we concluded that the first and fourth oxidations are twice as intense as the second and third. Taking this into account the first and fourth oxidation at +0.14 and +0.53 V corresponds to a global two-electron transfer, which was identified by the shapes of the CV and RDV curves as two overlapping reversible one-electron transfers. The second and third oxidation at +0.26 and +0.39 V, respectively, are reversible one-electron transfers. In addition, four oxidation steps could be observed for **G1** (Table 1, see the Supporting Information). As it is expected that all 12 nitrogen-centers are oxidized, it seems reasonable to assume that each step involves three electrons.

Due to the symmetric nature of **MC6** and **G1**, it is not possible to determine the exact localization of the electron transfers. Considering the relatively small potential separations of the oxidation processes in **MC6** and **G1**, a moderate communication between the DTPA subunits is assumed which is furthermore confirmed by decreased first oxidation potentials compared with the single DTPA unit that is reversibly oxidized at +0.34 V (Table 1).

The HOMO levels of **MC6** (−4.94 eV) match well with the work function of metallic gold (−5.1 eV), which could potentially enhance the hole charge injection between the electrode and the semiconducting material in FETs or OLEDs, and thus improve the device performance.[46,59,60]

DFT calculations (B3LYP/6-31G*)[61] carried out on **MC6** (E_{HOMO}^{DFT} = −4.28 eV) revealed a totally symmetric HOMO level which is in fairly good agreement with the electrochemical investigations (Figure 8, bottom, see the Supporting Information for the respective LUMO level). Contributions of the central nitrogen atoms as well as the internal and exocyclic phenyl rings were thereby observed.

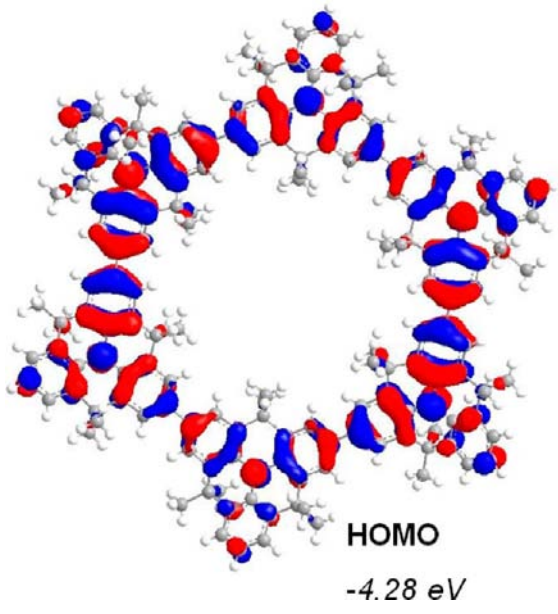

Figure 8. HOMO of **MC6** calculated by DFT (B3LYP/6-31G*). See the Supporting Information for the calculated LUMO.

dx.doi.org/10.1021/ja400857g | J. Am. Chem. Soc. 2013, 135, 4550−4557

CONCLUSIONS

In summary, we have successfully fabricated a π-conjugated DTPA macrocycle by two different synthetic concepts. By analyzing the solution-based and surface-mediated one-step synthesis starting from the same precursor, a preference for the macrocyclization compared to the zigzag conformation on surface is revealed. This observation is attributed to the confinement of the DTPA molecules to two dimensions upon on-surface synthesis, which reduces their conformational and orientational degrees of freedom compared to the situation in solution. To investigate the properties of the DTPA macrocycle, we subsequently synthesized **MC6** by a stepwise protocol in solution. Single-crystal X-ray analysis confirmed the successful cyclization. Bromination of **MC6** allowed furthermore the extension toward expanded macrocycles **G1** and **G2**. The comparative study of the optical properties of **MC6**, **G1** and **G2** with linear nonamer **L9** and the parent DTPA revealed differences that could be correlated to the cyclic nature of the species. They showed a deep blue emission in solution together with a significant improvement in the PLQY with respect to DTPA as a result of the extended π-conjugation along the cyclic backbone. Due to the matching HOMO level with the work function of metallic gold, the good solubility and the environmental stability of **MC6**, it could be applied as hole-transport layer in OFETs and OLEDs. Studies on these topics are currently being pursued in our group.

ASSOCIATED CONTENT

Supporting Information

Experimental details, crystallographic data for **MC6** (CIF), NMR, MALDI-TOF MS as well as RDV, GPC, TGA and DSC curves. This material is available free of charge via the Internet at http://pubs.acs.org.

AUTHOR INFORMATION

Corresponding Author

muellen@mpip-mainz.mpg.de; roman.fasel@empa.ch

Notes

The authors declare no competing financial interest.

ACKNOWLEDGMENTS

This work was supported by the Transregio SFB TR49 (Frankfurt, Mainz, Kaiserslautern), the Swiss National Science Foundation (SNSF) and the Alexander von Humboldt Foundation (postdoctoral fellowships to M.K.). We are grateful to Dr. Manfred Wagner and Dr. Tomohiko Nishiuchi for the help with the NMR measurements and DFT calculations.

REFERENCES

(1) Iyoda, M. *Pure Appl. Chem.* **2010**, *82*, 831−841.
(2) Iyoda, M.; Yamakawa, J.; Rahman, M. J. *Angew. Chem., Int. Ed.* **2011**, *50*, 10522−10553.
(3) Jung, S. H.; Pisula, W.; Rouhanipour, A.; Räder, H. J.; Jacob, J.; Müllen, K. *Angew. Chem., Int. Ed.* **2006**, *45*, 4685−4690.
(4) Pisula, W.; Kastler, M.; Yang, C.; Enkelmann, V.; Müllen, K. *Chem.-Asian J.* **2007**, *2*, 51−56.
(5) Blunt, M. O.; Russell, J. C.; Gimenez-Lopez, M. D.; Taleb, N.; Lin, X. L.; Schroder, M.; Champness, N. R.; Beton, P. H. *Nat. Chem.* **2011**, *3*, 74−78.
(6) Tahara, K.; Yamaga, H.; Ghijsens, E.; Inukai, K.; Adisoejoso, J.; Blunt, M. O.; De Feyter, S.; Tobe, Y. *Nat. Chem.* **2011**, *3*, 714−719.
(7) Chen, P. K.; Jäkle, F. *J. Am. Chem. Soc.* **2011**, *133*, 20142−20145.
(8) Chen, P. K.; Lalancette, R. A.; Jäkle, F. *Angew. Chem., Int. Ed.* **2012**, *51*, 7994−7998.
(9) Ito, A.; Yokoyama, Y.; Aihara, R.; Fukui, K.; Eguchi, S.; Shizu, K.; Sato, T.; Tanaka, K. *Angew. Chem., Int. Ed.* **2010**, *49*, 8205−8208.
(10) Grave, C.; Schlüter, A. D. *Eur. J. Org. Chem.* **2002**, 3075−3098.
(11) Höger, S. *Chem.—Eur. J.* **2004**, *10*, 1320−1329.
(12) Mössinger, D.; Chaudhuri, D.; Kudernac, T.; Lei, S.; De Feyter, S.; Lupton, J. M.; Höger, S. *J. Am. Chem. Soc.* **2010**, *132*, 1410−1423.
(13) Mössinger, D.; Hornung, J.; Lei, S.; De Feyter, S.; Höger, S. *Angew. Chem., Int. Ed.* **2007**, *46*, 6802−6806.
(14) Zhang, W.; Moore, J. S. *Angew. Chem., Int. Ed.* **2006**, *45*, 4416−4439.
(15) Shizu, K.; Sato, T.; Ito, A.; Tanaka, K.; Kaji, H. *J. Mater. Chem.* **2011**, *21*, 6375−6382.
(16) Zhang, J. S.; Pesak, D. J.; Ludwick, J. L.; Moore, J. S. *J. Am. Chem. Soc.* **1994**, *116*, 4227−4239.
(17) Tobe, Y.; Nagano, A.; Kawabata, K.; Sonoda, M.; Naemura, K. *Org. Lett.* **2000**, *2*, 3265−3268.
(18) Iwamoto, T.; Watanabe, Y.; Sadahiro, T.; Haino, T.; Yamago, S. *Angew. Chem., Int. Ed.* **2011**, *50*, 8342−8344.
(19) Hoffmann, M.; Wilson, C. J.; Odell, B.; Anderson, H. L. *Angew. Chem., Int. Ed.* **2007**, *46*, 3122−3125.
(20) Hoffmann, M.; Karnbratt, J.; Chang, M. H.; Herz, L. M.; Albinsson, B.; Anderson, H. L. *Angew. Chem., Int. Ed.* **2008**, *47*, 4993−4996.
(21) Höger, S.; Meckenstock, A. D.; Pellen, H. *J. Org. Chem.* **1997**, *62*, 4556−4557.
(22) Lovett, J. E.; Hoffmann, M.; Cnossen, A.; Shutter, A. T. J.; Hogben, H. J.; Warren, J. E.; Pascu, S. I.; Kay, C. W. M.; Timmel, C. R.; Anderson, H. L. *J. Am. Chem. Soc.* **2009**, *131*, 13852−13859.
(23) Franc, G.; Gourdon, A. *Phys. Chem. Chem. Phys.* **2011**, *13*, 14283−14292.
(24) Lackinger, M.; Heckl, W. M. *J. Phys. D: Appl. Phys.* **2011**, *44*, 464011.
(25) Mendez, J.; Lopez, M. F.; Martin-Gago, J. A. *Chem. Soc. Rev.* **2011**, *40*, 4578−4590.
(26) Palma, C. A.; Samori, P. *Nat. Chem.* **2011**, *3*, 431−436.
(27) Cai, J.; Ruffieux, P.; Jaafar, R.; Bieri, M.; Braun, T.; Blankenburg, S.; Muoth, M.; Seitsonen, A. P.; Saleh, M.; Feng, X.; Müllen, K.; Fasel, R. *Nature* **2010**, *466*, 470−473.
(28) Bieri, M.; Treier, M.; Cai, J.; Ait-Mansour, K.; Ruffieux, P.; Gröning, O.; Gröning, P.; Kastler, M.; Rieger, R.; Feng, X.; Müllen, K.; Fasel, R. *Chem. Commun.* **2009**, 6919−6921.
(29) Blunt, M. O.; Russell, J. C.; Champness, N. R.; Beton, P. H. *Chem. Commun.* **2010**, *46*, 7157−7159.
(30) Bieri, M.; Nguyen, M. T.; Groning, O.; Cai, J.; Treier, M.; Ait-Mansour, K.; Ruffieux, P.; Pignedoli, C. A.; Passerone, D.; Kastler, M.; Müllen, K.; Fasel, R. *J. Am. Chem. Soc.* **2010**, *132*, 16669−16676.
(31) Bieri, M.; Blankenburg, S.; Kivala, M.; Pignedoli, C. A.; Ruffieux, P.; Müllen, K.; Fasel, R. *Chem. Commun.* **2011**, *47*, 10239−10241.
(32) Lafferentz, L.; Ample, F.; Yu, H.; Hecht, S.; Joachim, C.; Grill, L. *Science* **2009**, *325*, 148−148.
(33) Lipton-Duffin, J. A.; Ivasenko, O.; Perepichka, D. F.; Rosei, F. *Small* **2009**, *5*, 592−597.
(34) Lafferentz, L.; Eberhardt, V.; Dri, C.; Africh, C.; Comelli, G.; Esch, F.; Hecht, S.; Grill, L. *Nat. Chem.* **2012**, *4*, 215−220.
(35) Gourdon, A. *Angew. Chem., Int. Ed.* **2008**, *47*, 6950−6953.
(36) Perepichka, D. F.; Rosei, F. *Science* **2009**, *323*, 216−217.
(37) Hellwinkel, D.; Melan, M. *Chem. Ber.* **1971**, *104*, 1001−1016.
(38) Hellwinkel, D.; Melan, M. *Chem. Ber.* **1974**, *107*, 616−626.
(39) Hellwinkel, D.; Melan, M.; Egan, W.; Degel, C. R. *Chem. Ber.* **1975**, *108*, 2219−2231.
(40) Hellwinkel, D.; Aulmich, G.; Melan, M. *Chem. Ber.* **1980**, *113*, 358−384.
(41) Shirota, Y.; Kageyama, H. *Chem. Rev.* **2007**, *107*, 953−1010.
(42) Wang, Y. J.; Sheu, H. S.; Lai, C. K. *Tetrahedron* **2007**, *63*, 1695−1705.
(43) Xu, B.; Fang, H. H.; Chen, F. P.; Lu, H. G.; He, J. T.; Li, Y. W.; Chen, Q. D.; Sun, H. B.; Tian, W. J. *New J. Chem.* **2009**, *33*, 2457−2464.

(44) Makarov, N. S.; Mukhopadhyay, S.; Yesudas, K.; Bredas, J. L.; Perry, J. W.; Pron, A.; Kivala, M.; Müllen, K. *J. Phys. Chem. A* **2012**, *116*, 3781−3793.
(45) Kan, E. J.; Hu, W.; Xiao, C. Y.; Lu, R. F.; Deng, K. M.; Yang, J. L.; Su, H. B. *J. Am. Chem. Soc.* **2012**, *134*, 5718−5721.
(46) Song, Y. B.; Di, C. A.; Xu, W.; Liu, Y. Q.; Zhang, D. Q.; Zhu, D. B. *J. Mater. Chem.* **2007**, *17*, 4483−4491.
(47) Nguyen, M. T.; Pignedoli, C. A.; Passerone, D. *Phys. Chem. Chem. Phys.* **2011**, *13*, 154−160.
(48) Yamamoto, T. *Bull. Chem. Soc. Jpn.* **1999**, *72*, 621−638.
(49) Yamamoto, T. *Prog. Polym. Sci.* **1992**, *17*, 1153−1205.
(50) Crystal data for **MC6** (CCDC 892865 contains the supplementary crystallographic data for this paper. These data can be obtained free of charge from The Cambridge Crystallographic Data Centre via www.ccdc.cam.ac.uk/data_request/cif.): Single crystals of **MC6** were obtained by slow diffusion of diethyl ether into a solution in chloroform. The unit cell contains 24 $CHCl_3$ molecules of which 16 are disordered. These have been treated as a diffuse contribution to the overall scattering without specific atom positions by SQUEEZE/PLATON (Spek, A. L. *J. Appl. Crystallogr.* **2003**, *36*, 7). Monoclinic, *C*2/*c*, a = 49.2578(9), b = 15.0524(6), c = 19.1141(7) Å, β = 101.6894(11)°. R = 0.0506, R_w = 0.0587.
(51) Walker, S. D.; Barder, T. E.; Martinelli, J. R.; Buchwald, S. L. *Angew. Chem., Int. Ed.* **2004**, *43*, 1871−1876.
(52) Barder, T. E.; Walker, S. D.; Jr, M.; Buchwald, S. L. *J. Am. Chem. Soc.* **2005**, *127*, 4685−4696.
(53) Do, K.; Kim, D.; Cho, N.; Paek, S.; Song, K.; Ko, J. *Org. Lett.* **2012**, *14*, 222−225.
(54) Fang, Z. Ph.D., National University of Singapore, 2008.
(55) Fang, Z.; Teo, T. L.; Cai, L. P.; Lai, Y. H.; Samoc, A.; Samoc, M. *Org. Lett.* **2009**, *11*, 1−4.
(56) Fang, Z.; Zhang, X. H.; Lai, Y. H.; Liu, B. *Chem. Commun.* **2009**, 920−922.
(57) Fang, Z.; Chellappan, V.; Webster, R. D.; Ke, L.; Zhang, T. F.; Liu, B.; Lai, Y. H. *J. Mater. Chem.* **2012**, *22*, 15397−15404.
(58) DigiElch v 6F, http://www.elchsoft.com/.
(59) Drolet, N.; Morin, J. F.; Leclerc, N.; Wakim, S.; Tao, Y.; Leclerc, M. *Adv. Funct. Mater.* **2005**, *15*, 1671−1682.
(60) Meijer, E. J.; de Leeuw, D. M.; Setayesh, S.; van Veenendaal, E.; Huisman, B. H.; Blom, P. W. M.; Hummelen, J. C.; Scherf, U.; Kadam, J.; Klapwijk, T. M. *Nat. Mater.* **2003**, *2*, 834−834.
(61) Frisch, M. J., et al. In *Gaussian 03*, Revision C.02; Gaussian, Inc.: Wallingford CT, 2004 (see the Supporting Information for a full citation).